Electrohydrodynamic Flow and Colloidal Patterning near Inhomogeneities on Electrodes

W. D. Ristenpart,† P. Jiang, M. A. Slowik, C. Punckt, D. A. Saville,‡ and I. A. Aksay*

Department of Chemical Engineering, Princeton University, Princeton, New Jersey 08544

Received May 7, 2008. Revised Manuscript Received July 15, 2008

Current density inhomogeneities on electrodes (of physical, chemical, or optical origin) induce long-range electrohydrodynamic fluid motion directed toward the regions of higher current density. Here, we analyze the flow and its implications for the orderly arrangement of colloidal particles as effected by this flow on patterned electrodes. A scaling analysis indicates that the flow velocity is proportional to the product of the applied voltage and the difference in current density between adjacent regions on the electrode. Exact analytical solutions for the streamlines are derived for the case of a spatially periodic perturbation in current density along the electrode. Particularly simple asymptotic expressions are obtained in the limits of thin double layers and either large or small perturbation wavelengths. Calculations of the streamlines are in good agreement with particle velocimetry experiments near a mechanically generated inhomogeneity (a "scratch") that generates a current density larger than that of the unmodified electrode. We demonstrate that proper placement of scratches on an electrode yields desired patterns of colloidal particles.

Introduction

Guided patterning of surfaces with colloidal particles is of interest for use in applications ranging from biosensors,[1] lab-on-a-chip devices,[2] optics,[3,4] and magnetic data storage.[5] To produce such patterns, our group demonstrated that the distribution of current across an indium tin oxide (ITO) electrode can be altered in the presence of an ultraviolet (UV) illumination motif; during the electrophoretic deposition process, the colloidal particles aggregate on the regions illuminated by the UV light.[6] Although the basis of this colloidal aggregation on the inhomogeneities generated by the UV light is not well understood, the process was thought to be related to the phenomenon of planar particle aggregation near electrodes in both steady and oscillatory fields.[7,8] The work presented here extends this process to particle agglomeration on inhomogeneities produced with physically patterned scratches on ITO and also provides a fundamental basis for the flows generated that lead into the colloidal aggregation process.

Trau et al.[7,9] studied the aggregation behavior of polystyrene and gold nanoparticles and proposed that the particles are carried toward one another by electrohydrodynamic (EHD) flow. In this model, the particles alter the local electric field near the electrode, and the action of these perturbations on the electrode polarization layer yields fluid motion directed toward each particle. Unlike classical electroosmosis, in which the mobile equilibrium charge in the fluid balances charge that is chemically bound to solid−liquid interfaces, here the charge in the fluid is proportional to the externally imposed potential. The electrical stresses scale nonlinearly with the field strength, and the resulting flow is denoted as EHD.[10] Other authors use other nomenclature, including "induced charge electroosmosis".[11] Provided the particles do not adhere to the electrode, adjacent particles become mutually entrained in their respective flows and aggregation ensues. Ristenpart et al.[12,13] developed more detailed models based on the EHD theory and found that measurements of the aggregation kinetics and direct flow visualization corroborated the theory for high frequency fields in the absence of faradaic reactions. Sides and co-workers expanded Trau et al.'s model for the case of low frequency oscillatory faradaic currents and found significant dependence on the nature of the electrolyte.[14−16] As for steady fields, Solomentsev et al.[17,18] proposed an alternative mechanism based on electroosmotic slip flow on the surface of the particle. Recent work by Ristenpart et al.[19] indicates that both EHD flow and electroosmotic flow (EOF) contribute significantly to aggregation in steady fields.

Although most research has focused on flow induced by the particles themselves, several results indicate that particles are not the only source of flow near electrodes. Trau et al. noted that any lateral potential gradient within the electrode polarization layer will yield fluid motion, and they tested this by preparing a glass slide half-coated with a thin layer of indium tin oxide (ITO).[9] Upon application of an electric field, particles moved away from the bare silica and toward the ITO. They interpreted this result in terms of EHD flow directed from the low field

* To whom correspondence should be addressed. Telephone: (609) 258-4393. E-mail: iaksay@princeton.edu.

† Current address: Department of Chemical Engineering and Materials Science and Department of Food Science and Technology, University of California, Davis, CA 95616.

‡ Deceased.

(1) Velev, O. D.; Kaler, E. W. *Langmuir* **1999**, *15*, 3693–3698.
(2) Gau, H.; Herminghaus, S.; Lenz, P.; Lipowsky, R. *Science* **1999**, *283*, 46–49.
(3) Lin, S.-Y.; Chow, E.; Hietala, V.; Villeneuve, P. R.; Joannopoulos, J. D. *Science* **1998**, *282*, 274–276.
(4) Painter, O. *Science* **1999**, *284*, 1819–1821.
(5) Haginoya, C.; Ishibashi, M.; Koike, K. *Appl. Phys. Lett.* **1997**, *71*, 2934–2936.
(6) Hayward, R. C.; Saville, D. A.; Aksay, I. A. *Nature* **2000**, *404*, 56–59.
(7) Trau, M.; Saville, D. A.; Aksay, I. A. *Science* **1996**, *272*, 706–709.
(8) Bohmer, M. *Langmuir* **1996**, *12*, 5747–5750.
(9) Trau, M.; Saville, D. A.; Aksay, I. A. *Langmuir* **1997**, *13*, 6375–6381.
(10) Saville, D. A. *Annu. Rev. Fluid Mech.* **1997**, *29*, 27–64.
(11) Squires, T. M.; Bazant, M. Z. *J. Fluid Mech.* **2004**, *509*, 217–252.
(12) Ristenpart, W. D.; Aksay, I. A.; Saville, D. A. *Phys. Rev. E* **2004**, *69*, 021405.
(13) Ristenpart, W. D.; Aksay, I. A.; Saville, D. A. *J. Fluid Mech.* **2007**, *575*, 83–109.
(14) Sides, P. J. *Langmuir* **2001**, *17*, 5791–5800.
(15) Kim, J.; Anderson, J. L.; Garoff, S.; Sides, P. J. *Langmuir* **2002**, *18*, 5387–5391.
(16) Fagan, J. A.; Sides, P. J.; Prieve, D. C. *Langmuir* **2006**, *22*, 9846–9852.
(17) Solomentsev, Y.; Bohmer, M.; Anderson, J. L. *Langmuir* **1997**, *13*, 6058–6068.
(18) Solomentsev, Y.; Guelcher, S. A.; Bevan, M.; Anderson, J. L. *Langmuir* **2000**, *16*, 9208–9216.
(19) Ristenpart, W. D.; Aksay, I. A.; Saville, D. A. *Langmuir.* **2007**, *23*, 4071–4080.

10.1021/la801419k CCC: $40.75
Published on Web 10/02/2008

strength region (the glass) toward the high field strength region (the conductive ITO). Similarly, Yeh et al. used photolithography to prepare an electrode coated with alternating stripes of a thermal oxide layer, and they showed that application of an electric field induced particles to aggregate preferentially on the areas of low oxide thickness.[20] They also concluded that the particles migrated toward areas of higher electric field strength, and they proposed an EHD mechanism similar to that of Trau et al. Subsequently, patterned electrodes with large grooves have been used to place particles in desired locations.[21−23] Strikingly, Brisson and Tilton reported that a "circular asperity" on the counter electrode induced yeast cells to aggregate preferentially underneath the asperity on the working electrode,[24] suggesting that the inhomogeneity need not be immediately adjacent to the electrode where the particles reside for preferential aggregation to occur.

The above examples used physical inhomogeneities to induce a local increase in field strength. In contrast, in the work by Hayward et al. on patterning with UV light, it was proposed that the UV light increases the rate at which electrons are promoted from valence to conduction bands within the semiconductive ITO.[6] This then yields a higher ionic current density in the fluid adjacent to the illuminated region, resulting in fluid motion directed toward the illumination. Flows induced by instabilities might also occur without any inhomogeneities present in the system, provided the current density is above the limiting current;[25] the colloidal aggregation experiments relevant here are typically performed well below the limiting current.

Although Trau et al.'s EHD mechanism is consistent with observations of particle motion toward regions of higher field strength, the theory has not been elaborated to provide quantitative information about the flow structure. Trau et al. performed numerical calculations of the flow induced on an electrode with a spatially sinusoidal current density,[9] but they assumed that the fluid is electroneutral to leading order and did not elaborate for other geometries. Pundik et al.[26] obtained qualitatively similar streamlines for the case of a nonflat electrode with an oscillatory height profile; for surface roughness on the order of nanometers, such flows should be negligible. Nadal studied the inverse problem where a thin dielectric strip is placed on a conductive electrode subject to an oscillatory field, and they proposed a model based on lateral gradients in the surface capacitance of a thin layer adjacent to the electrode.[27] They performed particle tracking experiments, and found satisfactory agreement with their theory, but the results are not directly applicable to gradients in electric field strength in steady (DC) fields with faradaic currents.

In this work, we present a more detailed investigation of the EHD flow induced near inhomogeneous electrodes in steady fields. The key (and perhaps counterintuitive) result is that the free charge in the double layer *decreases* in regions of higher current density, yielding a potential gradient directed toward the region of higher current density that provides the body force driving fluid motion. This result serves as the basis for a scaling expression describing the EHD flow velocity, wherein the electrode is modeled as a physically flat surface of constant potential but with varying current density. According to the model, the EHD velocity is linearly proportional to both the applied potential and the difference in current density between two adjacent regions, directed toward the region of higher current density (Figure 1).

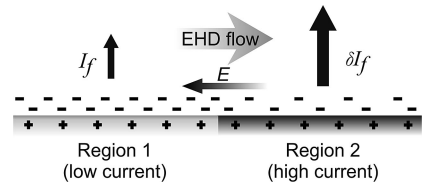

Figure 1. Sketch showing an electrode with different current densities in adjacent regions. The potential drop across the charge polarization layer is smaller in the region of higher current density, creating a lateral electric potential gradient and resulting in EHD flow toward the higher current density region. Note that the electric field E is not imposed externally but is the consequence of two adjacent regions with different current densities.

The paper is organized as follows: First, approximate scaling expressions are derived for the magnitude of the EHD flow in the context of the standard electrokinetic theory. The structure of the flow is then investigated via exact analytical solutions for the potential distribution and flow field, derived for the case of a spatially oscillatory current density along the electrode. Simple asymptotic expressions are obtained in various limiting regimes; for example, in the limit of thin double layers and long perturbation wavelengths, the lateral velocity varies quadratically between the electrodes. Since the governing equations are linear, current perturbations of different wavelengths can be superimposed (via a Fourier series) to generate arbitrary current distributions and their corresponding flow patterns. For the case of a thin strip of higher current density, two counter-rotating rolls are generated around the edges of the strip with the flow directed toward the strip along the electrode, consistent with the scaling theory and previous experimental observations.

Next, to test the model, we use video microscopy to conduct particle velocimetry experiments near "scratches" on ITO electrodes, where the scratches are produced by lightly dragging a razor blade across the ITO surface. Velocity profiles calculated from particle trajectories are in good agreement with the theoretical model, using one electrochemical fitting parameter. Although the electrochemistry associated with the scratches is not well characterized, scanning electron microscopy (SEM) and atomic force microscopy (AFM) images suggest that the granular ITO film undergoes densification within the scratch and that the surface roughness is decreased. Consequently, the ITO surface is more conductive locally, consistent with the increased current density observed experimentally.

Finally, we demonstrate that proper placement of scratches on the electrode yields a desired pattern of colloidal particles on the electrode, and we discuss how this approach can serve as the basis for fabrication of more complicated patterns.

Theory

Governing Equations. The theory is based on the standard electrokinetic model as set out by Russel et al.,[28]

$$0 = -\nabla P - e\left(\sum_i \nu_i n_i\right)\mathbf{E} + \mu\nabla^2\mathbf{u} \tag{1}$$

$$\nabla\cdot\mathbf{u} = 0 \tag{2}$$

$$\frac{\partial n_i}{\partial t} = D_i\nabla^2 n_i + e\nu_i\frac{D_i}{k_B T}\nabla\cdot(n_i\nabla\phi) - \mathbf{u}\cdot\nabla n_i, \tag{3}$$

(20) Yeh, S. R.; Seul, M.; Shraiman, B. I. *Nature* **1997**, *386*, 57–59.
(21) Kumacheva, E.; Golding, R. K.; Allard, M.; Sargent, E. H. *Adv. Mater.* **2002**, *14*, 221–224.
(22) Golding, R. K.; Lewis, P. C.; Kumacheva, E. *Langmuir* **2004**, *20*, 1414–1419.
(23) Choi, W. M.; Park, O. *Nanotechnology* **2006**, *17*, 325–329.
(24) Brisson, V.; Tilton, R. D. *Biotechnol. Bioeng.* **2002**, *77*, 290–295.
(25) Zaltzman, B.; Rubinstein, I. *J. Fluid Mech.* **2007**, *579*, 173–226.
(26) Pundik, T.; Rubinstein, I.; Zaltzman, B. *Phys. Rev. E* **2005**, *72*, 061502.
(27) Nadal, F. *Eur. Phys. J. E* **2002**, *9*, 387–399.
(28) Russel, W. B.; Saville, D. A.; Schowalter, W. R. *Colloidal Dispersions*, 1st ed.; Cambridge University Press: Cambridge, U.K., 1991.

$$-\varepsilon\varepsilon_0\nabla^2\phi = \rho^{(f)} = e\sum_i \nu_i n_i \tag{4}$$

Here, P is pressure, e is the charge on a proton, n_i is the number density of ions with valence ν_i and diffusivity D_i, $\mathbf{E} = -\nabla\phi$ is the electric field strength, μ is the viscosity, $\mathbf{u}$ is the fluid velocity, k_BT is the product of Boltzmann's constant and the absolute temperature, ε is the dielectric constant of the liquid, and ε_0 is the permittivity of free space. Equation 1 represents the momentum balance in the limit of negligible inertia, with an electric body force term. The number densities of ions are related to the electric potential through Gauss's equation (eq 4) and also by the conservation relation expressed in eq 3. Here, the flux of ions is prescribed by the Nernst−Planck equation; the three terms on the right-hand side of eq 3 represent diffusion, electromigration, and convection, respectively.

This model has been studied in detail for isolated spheres,[29,30] and it served as the starting point for analyses of particles near electrodes in oscillatory[12,13] and steady fields[19] by Ristenpart et al. Here, we use the model in the steady-field situation (with a faradaic flux) to analyze the effect of lateral perturbations in the current density along the electrode. The unperturbed case has been described previously;[19] we briefly summarize that analysis before analyzing the effects of lateral perturbations in the current density.

Two parallel electrodes, separated by a distance $2H$ with the center line at $y = 0$, are subjected to a steady potential difference $\Delta\phi$. In the absence of lateral (x-direction) perturbations, the velocity is zero everywhere and osmotic pressure balances the electrostatic body force. The flux of ions at each electrode depends on the nature of the electrochemical reactions; for convenience, we assume that a monovalent charged species is produced and consumed at the respective electrodes and that its concentration is much less than that of a monovalent supporting electrolyte. (This situation is typical of water electrolysis, one of the main reactions studied experimentally.) Denoting species 1 as the cationic ion involved in the electrochemical reaction, the flux according to the Nernst−Planck equation is

$$I_f = ej_1 = -eD_1\frac{\mathrm{d}n_1}{\mathrm{d}y} - \frac{e^2D_1n_1}{k_BT}\frac{\mathrm{d}\phi}{\mathrm{d}y} \tag{5}$$

where I_f is the current resulting from the faradaic reactions at the electrodes. The fluxes of the other ionic species, which are neither consumed nor produced at the electrodes, are identically zero. The current density I_f depends on a number of factors, including the applied potential, the type of electrodes, and the ionic concentrations,[31] but we generalize the treatment by treating the current as an independent parameter rather than restricting our analysis to any specific kinetic model. We emphasize that the current is not truly independent of the applied potential (and is clearly constrained by the sign of the potential and the limiting current), but a more detailed model is not necessary to determine the resulting hydrodynamics. As discussed by Ristenpart et al.,[19] the transient nature of potentiostatic and galvanostatic systems may be neglected if the characteristic time scale for the electrochemistry obeys the inequality $t^* \gg H^2/D_i$, which is satisfied for most systems of interest.

The remaining boundary conditions involve specification of the potential at each electrode and a symmetry condition such that the charge density vanishes at the center line (which prevents the formation of asymmetrical charge distributions in steady-state systems). Linearization following the procedure outlined previously[19] yields the solution

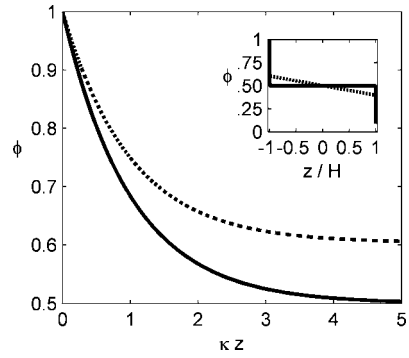

Figure 2. Dimensionless electric potential between parallel electrodes for a steady applied potential difference resulting in different faradaic current densities: solid line, $I_f = 0$; dotted line, $I_f = 100\ \mu\mathrm{A/cm^2}$. The potential drop across the polarization layer is smaller for the higher current density. Inset: the dimensionless potential across the entire cell, showing that the potential drop occurs mostly over the polarization layers near each electrode (not resolvable at this scale). Parameters: $\kappa^{-1} = 10$ nm, $H = 100\ \mu$m, and $\Delta\phi = 1$ V.

$$\phi = \frac{\Delta\phi}{2}\left(1 - \frac{\sinh\kappa y}{\sinh\kappa H}\right) - \frac{I_fH}{\sigma_\infty}\left(\frac{y}{H} - \frac{\sinh\kappa y}{\sinh\kappa H}\right) \tag{6}$$

$$\rho^{(f)} = \frac{e^2n_2^\infty}{k_BT}\left(\Delta\phi - \frac{I_fH}{\sigma_\infty}\right)\frac{\sinh\kappa y}{\sinh\kappa H} \tag{7}$$

Here, the Debye length is $\kappa^{-1} = (\varepsilon\varepsilon_0k_BT/2e^2n_2^\infty)^{1/2}$, and the bulk conductivity is $\sigma_\infty = 2e^2D_1n_2^\infty/k_BT$. Several features of the potential and charge distributions deserve mention. The first term in eq 6 is equivalent to the Goüy−Chapman model[28] between parallel plates, with the potential decaying exponentially near each electrode. For $\kappa H \gg 1$ and absent a faradaic reaction, the potential drop occurs entirely across the polarization layers near the electrodes, and the electric field strength in the bulk is zero. The second term describes the effect of the faradaic current on the potential. For applied potentials above the redox potential, I_f is nonzero and the field strength well away from the electrodes is approximated by Ohm's law,

$$E = -\frac{\mathrm{d}\phi}{\mathrm{d}y} \cong \frac{I_f}{\sigma_\infty}, \quad y \to 0 \tag{8}$$

Although the faradaic current increases the electric field strength outside the polarization layers, inside the layers the opposite is true: the field strength (and charge density) decreases as the current is increased (Figure 2). Near the positive electrode, positive ions are injected by the faradaic flux into the negatively charged polarization layer, decreasing the total charge (and field strength). At the opposite electrode, positive ions are removed from the positively charged polarization layer, again decreasing the charge and field strength. As we shall see, the decrease in potential with increasing current provides the necessary field imbalance to drive EHD flow between regions with different current densities. For $\kappa H \gg 1$, the (area) charge density in the polarization layer near each electrode is

$$q = -\varepsilon\varepsilon_0\frac{\mathrm{d}\phi}{\mathrm{d}y} \cong \pm\varepsilon\varepsilon_0\kappa\left(\frac{\Delta\phi}{2} - \frac{I_fH}{\sigma_\infty}\right), \quad y \to \pm H \tag{9}$$

Scaling Analysis for EHD Flow. To examine the EHD flow arising from a current inhomogeneity on an electrode, we follow an analysis similar to that used for spherical colloids in steady

(29) O'Brien, R. W.; White, L. R. *J. Chem. Soc., Faraday Trans. 2* **1978**, *74*, 1607–1626.
(30) Delacey, E. H. B.; White, L. R. *J. Chem. Soc., Faraday Trans. 2* **1981**, *77*, 2007–2039.
(31) Newman, J. *Electrochemical Systems*, 1st ed.; Prentice-Hall: Englewood Cliffs, NJ, 1973.

fields.[19] Variations in the faradaic current density at the electrode perturb the otherwise uniform field, inducing a force on the charge in the polarization layer and creating flow. The relation between the tangential electrical stresses and velocity is expressed by the Helmholtz−Smoluchowski equation for steady electroosmosis in a diffuse layer along a rigid, charged interface.[28] Within the charge layer, electrical stresses are balanced by viscous shear, while outside the Debye layer the fluid velocity asymptotes to the Helmholtz−Smoluchowski value,

$$u^* = \frac{\varepsilon\varepsilon_0\Delta\phi}{\mu}E_t \tag{10}$$

Here, $\Delta\phi$ is the electrostatic potential at the electrode solid−fluid interface and E_t is the tangential component of the applied electric field. For a negatively charged surface, $\Delta\phi < 0$, and the action of the field on positively charged counterions produces fluid motion in the direction of the field. It is useful to rewrite this expression using Gauss's law to relate the potential gradient and q, the total charge per unit area in the diffuse layer, as a balance between the electric and viscous stresses on the Debye scale, that is,

$$\mu\frac{u^*}{\kappa^{-1}} = -\frac{\varepsilon\varepsilon_0\zeta}{\kappa^{-1}}E_t = qE_t \tag{11}$$

According to eq 11, the induced velocity is proportional to the electrical stress per unit area, qE_t.

As a first approximation for the EHD flow, we assume that an otherwise homogeneous electrode has a region where the local current density is increased (or decreased) by a factor $\delta \equiv I_f^{(2)}/I_f^{(1)}$ over a width Δx. The exact mechanism that produces the current difference is unimportant, provided that the electrode surface remains geometrically flat and is an equipotential. (Note that for perfectly conductive electrodes, the electric field within the electrode itself is identically zero and the potential is uniform.) A more detailed analysis would include the effects of thin insulating layers of varying thickness or capacitance across the electrode, but here we focus on the simplest case possible to elucidate the underlying physics.

In general, convection affects the ion concentration, but we limit our analysis to situations where the Péclet number is small, $\mathrm{Pe} = uH/D \ll 1$. When this condition is satisfied, and if the current densities in both regions are small enough such that $I_f \ll \sigma_\infty\Delta\phi/2H$, then by eq 9 the charge density along the electrode is approximately

$$q \sim -\varepsilon\varepsilon_0\kappa\Delta\phi/2 \tag{12}$$

To estimate the tangential electric field, we neglect the interaction between the two regions and approximate the potential in each region using eq 6. The tangential field is then

$$E_t \sim -\left(\frac{\phi_2-\phi_1}{\Delta x}\right) \sim \frac{-1}{\Delta x}\left[\frac{I_f H}{\sigma_\infty}\left(\frac{y}{H}-\frac{\sinh\ \kappa y}{\sinh\ \kappa H}\right)-\delta\frac{I_f H}{\sigma_\infty}\left(\frac{y}{H}-\frac{\sinh\ \kappa y}{\sinh\ \kappa H}\right)\right] \tag{13}$$

yielding

$$E_t \sim (\delta-1)\frac{I_f H}{\sigma_\infty\Delta x} \tag{14}$$

We ignore the y-dependence to focus on the scaling. Note that the component of the potential proportional to $\Delta\phi$ in eq 6 canceled out, leaving only the difference in potential due to the varied current density. Combining eqs 11, 12, and 14, it follows that the tangential EHD velocity scales as

$$\mathbf{u}\cdot\mathbf{t} \sim (\delta-1)\frac{\varepsilon\varepsilon_0\Delta\phi\mathrm{I}_f H}{2\mu\sigma_\infty\Delta x} \tag{15}$$

The flow is proportional to the product of the potential and current and is directed toward the region with the larger current density. For $\delta > 1$, the flow is directed toward region 2, otherwise toward region 1. If the currents are equal ($\delta = 1$), no flow occurs. Although the applied potential and current density are signed quantities, they are not independent. The direction of the flow is unchanged upon reversal of the polarity, consistent with the designation of the flow as electrohydrodynamic. Substitution of magnitudes typical for water electrolysis yields the velocity $u \approx 345(\delta-1)\ \mu$m/s, indicating that small current density variations yield significant flows. (For our experiments with deionized water, $\sigma_\infty \approx 1\ \mu$S/cm, $\Delta\phi \approx 1$ V, $I_f \approx 1\mu$A/cm^2, $H \approx 100\ \mu$m, and we estimate $\Delta x \approx 10\ \mu$m.)

Two aspects of eq 15 deserve attention. First, the magnitude of the EHD flow necessarily changes with time, since the applied potential and current density cannot simultaneously be held constant (because electrochemical cells are either potentiostatic or galvanostatic). For example, under potentiostatic conditions, the current typically decreases with time, so the observed fluid velocity will decrease in tandem. The flow is pseudosteady, however, provided $t^* \gg H^2/D_i$. Second, the EHD flow scales nonlinearly with the electric field strength, but the degree of nonlinearity depends on the functional relation between the applied potential difference and the corresponding current density. For applied potentials near the redox potential, the current varies linearly with the potential so the resulting EHD flow scales as E^2, but for larger potential differences the current often varies exponentially (e.g., the Tafel equation). In this situation, the EHD flow scales as $E \log E$.

Perturbation Analysis. To investigate the flow structure around current inhomogeneites, we use a perturbation method following the approach employed by Trau et al.[9] The key difference is that here we are armed with an exact solution to the (linearized) governing equations for the unperturbed potential distribution between the electrodes, whereas Trau et al. assumed the fluid was electroneutral to leading order.[9] This allows us to obtain an exact analytical solution for the flow streamlines for arbitrary values of κH and the perturbation wavelength.

As in the unperturbed case, we examine two electrodes separated by a distance $2H$, with $y = 0$ at the center line. In the limit of low Péclet number, the potential distribution is uncoupled from the hydrodynamics; thus, we solve the electrostatics and hydrodynamics sequentially. The electrostatic governing equations (eqs 3 and 4) and potential boundary conditions remain unchanged, but we assume that the current density is subject to a spatially oscillatory perturbation,

$$e\mathbf{j}_1\cdot\mathbf{n} = I_f + \tilde{I}_f\, e^{i\lambda x} \tag{16}$$

Here, $\lambda = 2\pi/L$, with L being the wavelength of the perturbation. Accordingly, the potential and charge densities are

$$\phi(x,y) = \phi(y) + \tilde{\phi}(y)\, e^{i\lambda x}$$
$$n_i(x,y) = n_i(y) + \tilde{n}_i(y)\, e^{i\lambda x} \tag{17}$$

Choosing scaling parameters $\tilde{\phi} \sim k_BT/e$, $\tilde{n}_i \sim n_i^\infty$, $y \sim H$, $x \sim \lambda^{-1}$, and $\tilde{I}_f \sim eD_1n_2^\infty/H$, upon linearization (i.e., neglecting terms proportional to the product $\tilde{\phi}\tilde{n}_i$) the dimensionless governing equations for the perturbation variables simplify to

$$\frac{\partial^2 \tilde{n}}{\partial y^2} = [(\kappa H)^2 + (\lambda H)^2]\tilde{n} \tag{18}$$

$$\frac{\partial^2 \tilde{\phi}}{\partial y^2} - (\lambda H)^2 \tilde{\phi} = -\frac{(\kappa H)^2}{2}\tilde{n} \tag{19}$$

Here, $\tilde{n} \equiv (n_1^\infty/n_2^\infty)\tilde{n}_1 + \tilde{n}_2 - \tilde{n}_3$ is the dimensionless total ion density. The boundary conditions for the perturbation variables are

$$\tilde{\phi} = 0, \quad y = \pm 1 \tag{20}$$

$$-2\frac{\partial \tilde{\phi}}{\partial y} - \frac{\partial \tilde{n}}{\partial y} = \tilde{I}_f, \quad y = -1 \tag{21}$$

$$\tilde{n} = 0, \quad y = 0 \tag{22}$$

The final boundary condition prevents asymmetrical charge distributions in steady-state systems.

Integration of eq 18 allows solution of eq 19 by variation of parameters, and application of boundary conditions 20−22 yields the dimensionless potential and density

$$\tilde{\phi} = \frac{\tilde{I}_f}{2\lambda H}\left[\tanh(\lambda H)\,\frac{\sinh(y\beta)}{\sinh(\beta)} - \frac{\sinh(y\lambda H)}{\cosh(\lambda H)}\right] e^{ix} \tag{23}$$

$$\tilde{n} = -\frac{\tilde{I}_f}{\lambda H}\left[\tanh(\lambda H)\,\frac{\sinh(y\beta)}{\sinh(\beta)}\right] e^{ix} \tag{24}$$

where $\beta^2 \equiv (\kappa H)^2 + (\lambda H)^2$. As in the unperturbed case, for $\kappa H \gg 1$, the charge density perturbation decays exponentially in the polarization layer near each electrode. The potential dependence is complicated by the second length scale λ^{-1}, but for $\lambda H \gg 1$, the potential drop is largely confined to the polarization layers as well.

Next, we address the hydrodynamics using the Stokes equations modified by an EHD body force, compare eqs 1 and 2. Because the problem is two-dimensional, we employ a stream function defined as

$$u_x = \frac{\partial \Psi}{\partial y}, \quad u_y = -\frac{\partial \Psi}{\partial x} \tag{25}$$

$$\Psi(x, y) = \Psi(y)\, e^{i\lambda x} \tag{26}$$

Substitution of eq 26 into eq 1 yields the inhomogeneous fourth order equation

$$\Psi'''' - 2(\lambda H)^2\Psi'' + (\lambda H)^4\Psi = i\lambda H[(\tilde{\phi}'' - (\lambda H)^2\tilde{\phi})\phi' - \tilde{\phi}\phi'''] \tag{27}$$

where the stream function has been scaled by $\Psi \sim \varepsilon\varepsilon_0(kT/e)^2/\eta$ and the primes denote differentiation with respect to y. Note that the right-hand side of eq 27 involves only known functions of y, so variation of parameters may be employed. Enforcing no-slip and no-penetration boundary conditions at the electrodes yields

$$\Psi = \Psi' = 0, \quad y = \pm 1 \tag{28}$$

The solution for the stream function to leading order is

$$\Psi = C_1 \sinh(y\lambda H) + C_2 y \cosh(y\lambda H) + K_1 \sinh(y\beta) + K_2 \cosh(y\lambda H)\sinh(y\kappa H) + K_3 \sinh(y\lambda H)\cosh(y\kappa H) \tag{29}$$

where the constants C_1, C_2, K_1, K_2, and K_3 are lengthy expressions that depend on the system parameters (i.e., λH, κH, $\Delta\phi$, I_f, and $\tilde{I}_f$). The full details are presented in the Supporting Information. Clearly, the general solution is quite complicated, so we gain intuition by examining specific limiting regimes.

Under typical experimental conditions, the Debye length is on the order of tens of nanometers, while the electrode separation may be micrometers to millimeters, so $\kappa H \gg 1$. If the homogeneous current density satisfies the inequality $I_f \ll \sigma_\infty \Delta\phi/2H$, then terms proportional to the homogeneous current density I_f are negligible. Under these conditions, it is instructive to examine two limits for the perturbation wavelength. For very long wavelengths ($\lambda H \ll 1$), eq 29 simplifies (in dimensional terms) to

$$\Psi \approx i\frac{\varepsilon\varepsilon_0\Delta\phi\tilde{I}_f\lambda H^2}{8\eta\sigma_\infty}\left(\frac{y^3}{H^3} - \frac{y}{H}\right)e^{i\lambda x} \tag{30}$$

with corresponding x-velocity

$$u_x \approx i\frac{\varepsilon\varepsilon_0\Delta\phi\tilde{I}_f\lambda H}{8\eta\sigma_\infty}\left(\frac{3y^2}{H^2} - 1\right)e^{i\lambda x} \tag{31}$$

Note that the prefactor in this latter expression matches the scaling predicted by eq 15, with $\Delta x = \lambda^{-1}$. Representative streamlines are presented in Figure 3A. Two counter-rotating rolls bisect the cell, with the flow along the electrodes directed toward the regions of highest current density. The x-velocity varies quadratically across the cell, with nonzero values at the electrodes. The

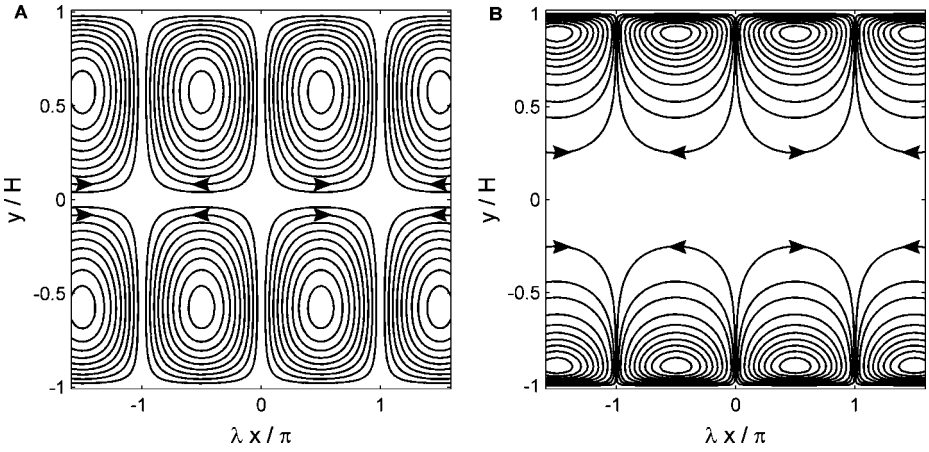

Figure 3. Streamlines for EHD flow between parallel electrodes subject to a spatially oscillatory perturbation in faradaic current density, in the thin double layer limit ($\kappa H = 10^3$). Arrows indicate direction of flow. (A) Long wavelength, $\lambda H = 10^{-2}$. Periodic counter-rotating rolls bisect the electrodes, with flow directed along the electrodes toward the regions of maximum current density. (B) Short wavelength, $\lambda H = 10$. Periodic counter-rotating rolls again bisect the electrodes, but the centers of circulation are closer to the electrodes.

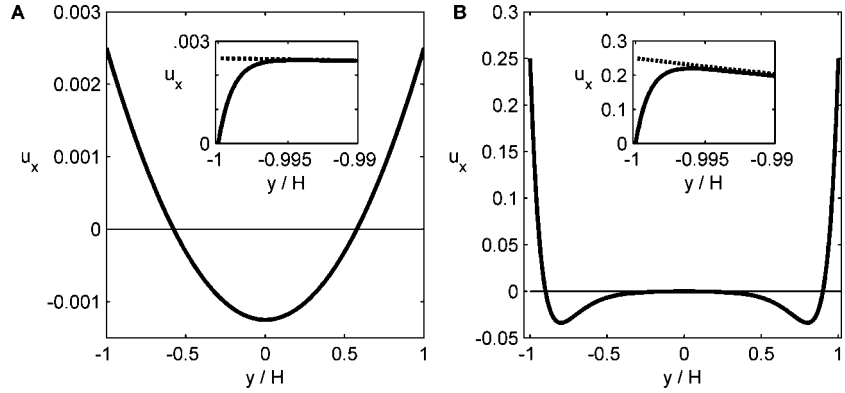

Figure 4. Dimensionless lateral (x-direction) velocities versus vertical position. Velocities extracted from the stream functions displayed in Figure 3, evaluated at $\lambda x = -\pi/2$ with $\kappa H = 10^3$. Positive velocities are in the positive x-direction. (A) Long wavelength, $\lambda H = 10^{-2}$. The flow varies quadratically between the electrodes; the exact velocity and asymptotic approximation (eq 31) are not differentiable at this scale. Inset: the exact (solid line) and asymptotic (dotted line) velocities very close to the electrode. The asymptotic expression misses the sharp decay to zero in the charge polarization layer. (B) Short wavelength, $\lambda H = 10$. The flow varies between the electrodes following eq 33, which again is not differentiable at this scale from the exact solution. Inset: exact (solid line) and asymptotic (dotted line) velocities very close to the electrode.

Table 1. Asymptotic Expressions for the Stream Function Derived from eq 29 and the Corresponding x-Direction Velocity[a]

Restriction	Stream Function	x-Velocity
$\kappa H >> \lambda H >> 1$	$\langle\Psi\rangle\left(\frac{(y/H)\mathrm{Cosh}(\lambda y)-\mathrm{Sinh}(\lambda y)}{\mathrm{Cosh}(\lambda H)}\right)$	$\langle u\rangle\left(\frac{(y/H)\mathrm{Sinh}(\lambda y)-\mathrm{Cosh}(\lambda y)}{\mathrm{Cosh}(\lambda H)}\right)$
$\lambda H >> \kappa H >> 1$	$\langle\Psi\rangle\frac{(\kappa H)^2}{(\lambda H)^2}\left(\frac{(y/H)\mathrm{Cosh}(\lambda y)-\mathrm{Sinh}(\lambda y)}{16\mathrm{Cosh}(\lambda H)}\right)$	$\langle u\rangle\frac{(\kappa H)^2}{(\lambda H)^2}\left(\frac{(y/H)\mathrm{Sinh}(\lambda y)-\mathrm{Cosh}(\lambda y)}{16\mathrm{Cosh}(\lambda H)}\right)$
$\kappa H >> 1,\ \lambda H << 1$	$\langle\Psi\rangle\frac{\lambda H}{8}\left(\frac{y^3}{H^3}-\frac{y}{H}\right)$	$\frac{\langle u\rangle}{8}\left(\frac{3y^2}{H^2}-1\right)$
$\kappa H << 1,\ \lambda H >> 1$	$\langle\Psi\rangle\left(\frac{2(y/H)\mathrm{Cosh}(\lambda y)-[(y/H)^2+1]\mathrm{Sinh}(\lambda y)}{32(\lambda H)^2\mathrm{Cosh}(\lambda H)/(\kappa H)^2}\right)$	$\langle u\rangle\left(\frac{2(y/H)\mathrm{Sinh}(\lambda y)-[(y/H)^2+1]\mathrm{Cosh}(\lambda y)}{32\lambda H\mathrm{Cosh}(\lambda H)/(\kappa H)^2}\right)$
$\kappa H << 1,\ \lambda H << 1$	$\langle\Psi\rangle\frac{\lambda H(\kappa H)^2}{480}\left(-\frac{y^5}{H^5}+\frac{2y^3}{H^3}-\frac{y}{H}\right)$	$\langle u\rangle\frac{(\kappa H)^2}{480}\left(-\frac{5y^4}{H^4}+\frac{6y^2}{H^2}-1\right)$

[a] All expressions are valid in the limit $I_f \ll \sigma_\infty\Delta\phi/2H$. $\langle\Psi\rangle \equiv i\varepsilon\varepsilon_0\Delta\phi\tilde{I}_f H e^{i\lambda x}/\mu\sigma_\infty$ and $\langle u\rangle \equiv \lambda\langle\Psi\rangle$.

approximate solution correctly captures the maximum magnitude of the flow near the electrode but misses the exponential decay within the double layer (Figure 4A, inset).

In the opposite limit of very short wavelengths, an approximate solution is obtained for the regime where $\kappa H \gg \lambda H \gg 1$. In this case, eq 29 simplifies to

$$\Psi \approx i\frac{\varepsilon\varepsilon_0\Delta\phi\tilde{I}_f H}{4\eta\sigma_\infty}\left(\frac{(y/H)\cosh(\lambda y)-\sinh(\lambda y)}{\cosh(\lambda H)}\right)e^{i\lambda x} \quad (32)$$

and the x-velocity is

$$u_x \approx i\frac{\varepsilon\varepsilon_0\Delta\phi\tilde{I}_f\lambda H}{4\eta\sigma_\infty}\left(\frac{(y/H)\sinh(\lambda y)-\cosh(\lambda y)}{\cosh(\lambda H)}\right)e^{i\lambda x} \quad (33)$$

As in the long wavelength case, the flow near each electrode is directed toward the regions of highest current density (Figure 3B), but the magnitude of the flow decays rapidly away from the electrodes. The velocity is essentially zero outside distances from the electrode much greater than λ^{-1}. The approximate solution accurately captures the shape of the velocity but again misses the rapid decay to zero within the charged layer (Figure 4B, inset). For the sake of completeness, we list asymptotic expressions for other limiting regimes in Table 1. Note, however, that many of these regimes are difficult to achieve experimentally.

A key feature of the preceding model is that the governing equation for the flow is linear (to leading order) with respect to the current density inhomogeneity. Consequently, we are free to superimpose current inhomogeneities with different wavelengths and magnitudes to investigate the flow resulting from specified current density patterns. Of most interest experimentally is the flow around a step inhomogeneity in current, of the form

$$\tilde{I}_f(x) = \begin{cases} \Delta I_f, & -w < x < w \\ 0, & |x| > w \end{cases} \quad (34)$$

In other words, the current density perturbation has magnitude ΔI_f inside a strip of width $2w$ and is zero elsewhere. To mimic this current density profile, we construct a rectangular wave using a Fourier series, namely

$$\tilde{I}_f/\Delta I_f = \frac{w}{L} + \sum_{n=1}^{n_{\mathrm{tot}}}\frac{2}{n\pi}\sin\left(\frac{n\pi w}{L}\right)\cos\left(\frac{n\pi x}{L}\right) \quad (35)$$

where L is the period of the waveform. Although this waveform is periodic, the choice of a sufficiently large period such that $L \gg w$ yields a flow near each inhomogeneity that is insensitive to L, that is, the waveform locally mimics the effect of a single inhomogeneity. Substitution of eq 35 into eq 29, and identifying $\lambda = n\pi/L$, yields a closed form analytical expression for the EHD

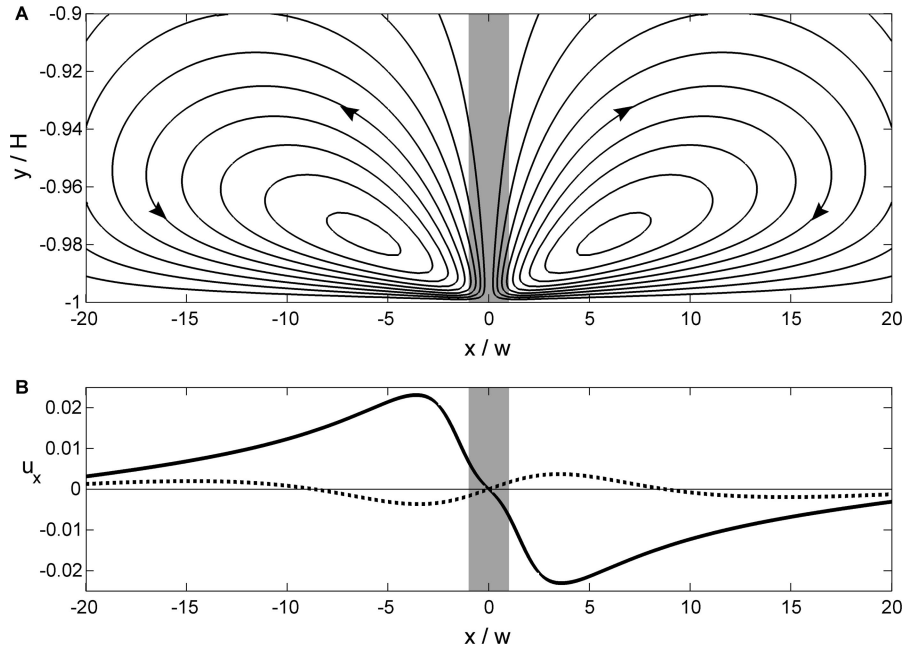

Figure 5. (A) Streamlines for EHD flow near a current inhomogeneity. The shaded region denotes the strip of width w in which the faradaic current is increased by a factor δ. A long-range flow is directed along the electrode toward the higher current density region. (B) Dimensionless lateral (x-direction) velocities, normalized by $\tilde{I}_f$, evaluated at $y/H = 0.995$ (solid line) and $y/H = 0.97$ (dotted line). Parameters: $\kappa H = 10^3$, $L/H = 0.5$, and $w/H = 10^{-2}$.

streamlines. For $w/L = 10^{-2}$, the solutions typically converged for values of $n_{tot} = 100$.

Figure 5 displays the predicted velocity profiles near a step current heterogeneity on the electrode surface. Two counter-rotating cells bisect the vicinity of the step heterogeneity, with the flow directed inward along the electrode surface. For sufficiently small heights above the electrode surface, fluid motion is directed toward the strip, while at larger heights the colloids are swept away (Figure 5B). Thus, colloids confined to the immediate vicinity of the electrode (i.e., by the electric field) are swept toward the current inhomogeneity.

Note that the direction of flow is controlled by the respective magnitudes of the current density inside and outside of the strip. If the current density were smaller in the strip compared to the rest of the electrode, then the shape of the streamlines in Figure 5A would be unchanged but with opposite direction.

Experimental Verification

Our theoretical results were tested by particle velocimetry experiments near "scratches" on glass slides coated with ITO (Delta Technologies, $R_s = 4-8\ \Omega$). Before each experiment, the ITO electrodes were cleaned by sonication in RBS detergent, thorough rinsing, and subsequent sonication in deionized water (Picopure). The aqueous colloidal polystyrene (PS) suspensions were purchased from Interfacial Dynamics Corporation, diluted, and cleaned by repeated centrifugation and dilution cycles with deionized water. The resulting conductivity of the suspension was 1 μS/cm.

Our experimental setup consisted of two parallel ITO electrodes. The distance between these was controlled by the thickness of a poly(dimethylsiloxane) (PDMS) spacer, which also confined the colloidal suspension in the space between the electrodes. Typical thicknesses ranged from 100 to 500 μm. Prior to the experiment, the bottom electrode was lightly scratched with a razor blade (cf., Figure 6A), while the top electrode was left unmodified. Power was supplied to the electrodes using a potentiostat (Princeton Applied Research), which allowed for simultaneous application of a potential and recording of the resulting current as a function of time. Comparative experiments with scratched and nonscratched electrodes indicated that the total current density on a scratched electrode was increased by a factor of 2 compared to unmodified electrodes (possible explanations for this will be given below).

Upon application of the field, particles immediately began moving laterally toward the scratch. After reaching the scratch, the particles typically became "stuck", that is, irreversibly adhered to the electrode, resulting in the preferential coverage of the scratched surface area (Figure 6B,C). Note that the electric field was oriented so that the negatively charged particles were attracted toward the electrode. Apparently, the field strength over the majority of the electrode was insufficient to induce sticking, whereas the higher electric field strength was sufficiently large. Likewise, this electrophoretic attraction and capture prevented the particles from moving upward, so recirculation up and away from the scratch was not observed.

To compare the experimentally obtained particle trajectories and the theoretical model described above, particle trajectories were analyzed using standard image analysis techniques in MatLab. The magnitude of the average particle velocity is plotted as a function of the lateral distance from the center of the scratch for different applied potentials in Figure 7. The particles clearly accelerate as they approach the scratch, qualitatively consistent with the streamlines shown in Figure 5. The solid lines show the theoretical predictions, using δ as the sole fitting parameter. The good agreement between experiment and theory is slightly impaired by an asymmetry in the experimental data for an applied potential of 1.75 V. This asymmetry might be caused by a small bulk electrolyte flow superimposing the flow pattern generated by the presence of the scratch. Likewise, the motion of particles less than 10 μm away from the center of the scratch could not be analyzed because particles tended to stick to the electrode surface across the whole width of the scratch (approximately 20 μm). Accordingly, the decrease in velocity close to the center of the scratch is not reflected in the experimental data. Nonetheless,

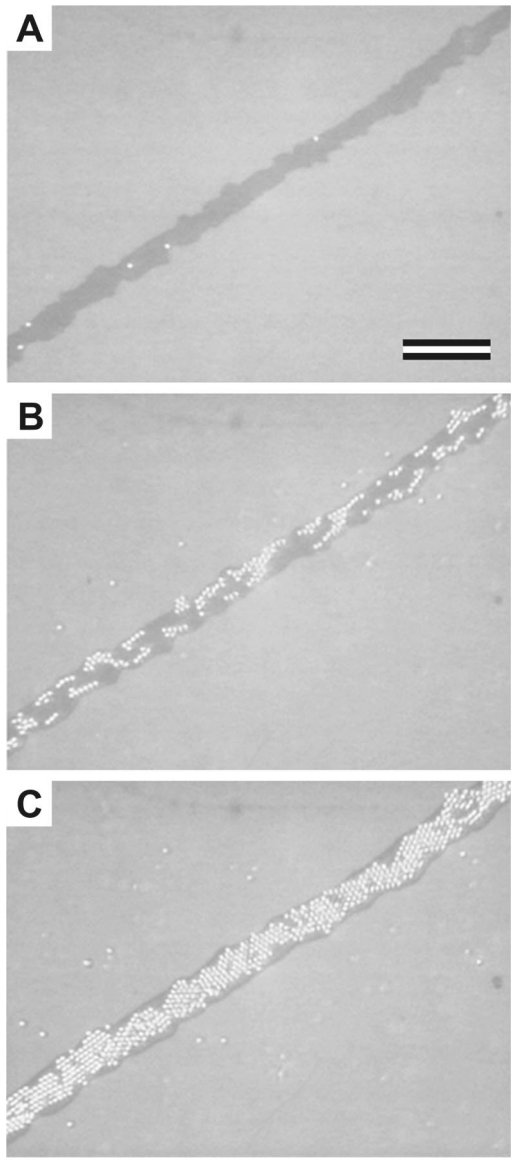

Figure 6. Preferential aggregation of particles along a scratch. Particles are 2.7 μm polystyrene suspended in deionized water with applied potential $\Delta\phi = 0.8$ V. Particles are white; scratch is dark. Scale bar is 30 μm. (A) Prior to application of the field, the particles are randomly dispersed. (B) At 30 s after application of the field, the particles have moved toward and aggregated preferentially along the scratch. (C) At 120 s after application of the field, the scratch is almost entirely covered by particles.

the model appears to capture the experimentally observed velocities everywhere else outside of the scratch.

Although the theoretical and experimental streamlines accord, some of the underlying details remain unclear. Most importantly, the model predicts that the velocity is proportional to the product of the applied potential and the current density difference, but this latter quantity could not be measured independently in our experimental setup. Moreover, the mechanism driving the increase in current density within the scratched surface area is not yet fully understood. Preliminary measurements with AFM indicate that the act of dragging or pressing the razor blade into the ITO causes a local densification and smoothing of the granular ITO (Figure 8A,B). The ITO film has a granular structure due to its fabrication process. Thus, the pressure exerted by the razor might yield local densification resulting in increased contact between the grains and thus increased surface conductivity and charge transport through the electrode−electrolyte interface. An alternative explanation could be the removal of an insulating surface layer during the scratching process.

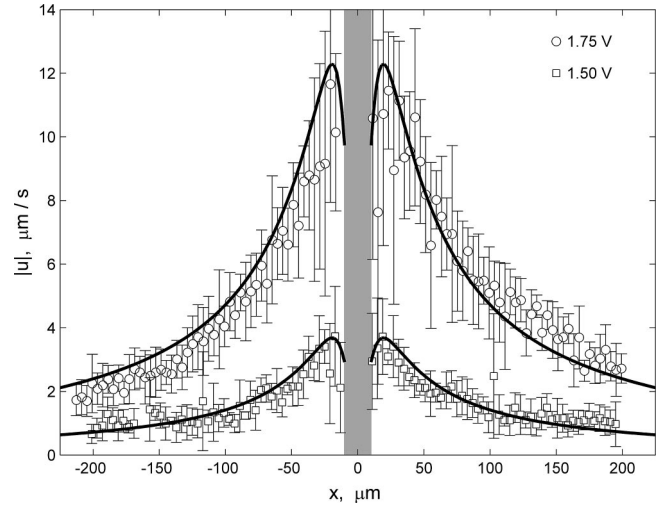

Figure 7. Comparison of experimental and predicted velocity profiles. A suspension of 2.4 μm PS particles in DI water was used. The applied potentials of 1.75 and 1.5 V correspond to electric fields of 33.0 V/cm and 28.3 V/cm, respectively. The measured current densities were 1 μA/cm^2 and 0.6 μA/cm^2, while the fit current density increases within the scratch were 0.07 μA/μm^2 and 0.02 μA/μm^2 respectively.

Regardless of the electrochemical details, the end result is that the current is dramatically increased (Figure 8C). When the applied electrical field was ramped from 0 to 3 V, an increase in current was observed as expected, but an electrode with a single scratch produced a current roughly twice as large as an unmodified electrode. Since the scratched area comprised a small fraction of the electrode area (at least, in terms of projected area), the local current density on the scratch must have been proportionally larger. For a 1 cm diameter electrode and a 20 μm wide scratch spanning the electrode, a crude estimate based on projected areas indicates that the current density is approximately 400 times greater in the scratch. The "electrochemical area" is typically much larger than the projected area because of surface roughness; however, effective electrode areas are typically measured using chronoamperometry on a redox species with a known diffusion coefficient.[32] This technique does not help identify the two different current densities here, since there is only one piece of information (the total current) but two unknown areas. More elaborate techniques will be necessary to measure the true current density versus position along the electrode.

A key observation is that if the pressure exerted on the razor was sufficiently large, then the ITO was completely "scraped" off of the glass substrate and no particle agglomeration was observed in the scratch. Rather, particles tended to accumulate at the edges of the scratch (data not shown). This behavior is consistent with the EHD model set forth here because the removal of the conductive layer necessarily causes the current density to vanish. Further work is necessary to elucidate optimal pressures for maximizing the increase in current density and the corresponding particle aggregation.

Although the electrochemical details are not well characterized, a key aspect of this phenomenon is the ease with which particles may be placed in desired locations and the ordering of particles that results there. After arriving at the scratch, the particles formed polycrystalline patches on the electrode surface (Figure 6C), consistent with particle-scale EHD and electroosmotic flows

(32) Kissinger, P. T.; Heineman, W. R. *Laboratory Techniques in Electroanalytical Chemistry*, 2nd ed.; Marcel Dekker: New York, 1996.

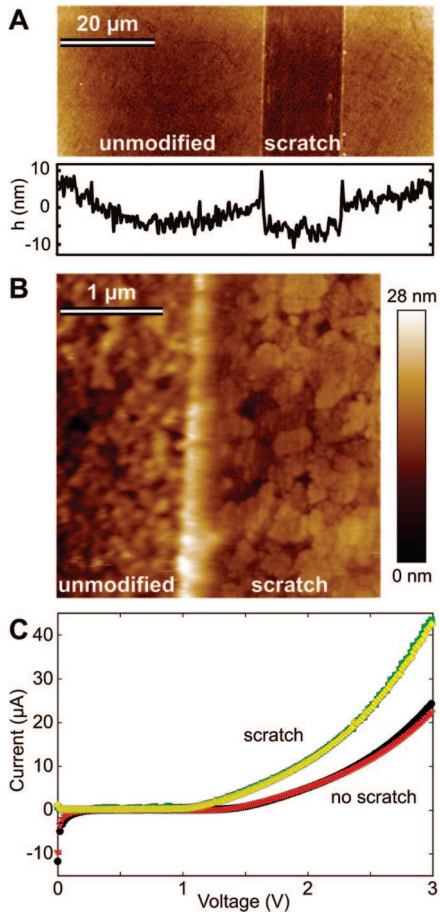

Figure 8. Atomic force microscopy images of a scratched ITO electrode and current response of scratched and unmodified electrodes. (A) Low magnification image. The darker region is the scratch. The horizontal profile below the image shows that the scratch is about 10 nm deep. (B) Higher magnification image of the left side of the scratch. Note that the average grain size in the unmodified region is smaller, while within the scratch the grains are larger, presumably due to compaction by the razor. (C) Current as a function of the applied voltage. Compared to an unmodified electrode (no scratch), the total current is almost doubled after a single scratch. Each experiment was performed twice (markers not differentiable at this scale).

which result in particle attraction and aggregation.[19] To achieve this result, we emphasize that nothing more than scratching the electrode lightly with a razor blade was required. This observation suggested that strategic placement of scratches on an electrode could be used to create arbitrary patterns of particles.

To test this idea, we patterned an ITO electrode with a regular lattice of scratches. This was accomplished simply by pressing a bundle of razor blades into the ITO, rotating the bundle by 90°, then pressing the bundle into the ITO again. In this fashion, a grid-shaped network of scratches was formed on the ITO. During an aggregation experiment, colloidal particles were attracted to the scratch pattern and formed close-packed polycrystalline layers on the surface (Figure 9). The particles thus assemble in predefined geometries on the electrode, suggesting that this approach will be useful for patterning electrodes with colloids.

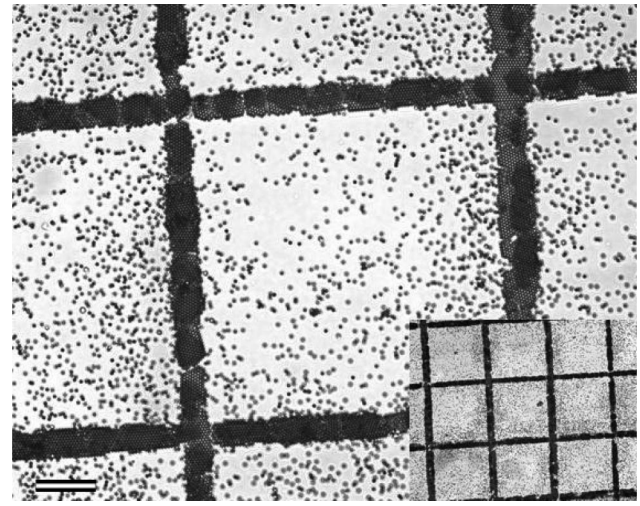

Figure 9. Optical microscopy image of 2.7 μm polystyrene particles aggregated preferentially on a network of scratches on an ITO electrode. Scale bar is 40 μm. Inset shows lower magnification of the same pattern.

Conclusions

We investigated EHD fluid motion near current heterogeneities on electrodes, and we demonstrated theoretically that the flow velocity is proportional to the applied voltage and the difference in current density. Streamlines of the flow were derived analytically for the case of a spatially oscillatory perturbation in current, and by appropriate superposition streamlines for the flow near a step heterogeneity (i.e., a scratch) were obtained. Our theoretical streamlines are in quantitative agreement with experiments using suspensions of PS particles in DI water with scratched ITO electrodes, with the use of one fitting parameter. More rigorous testing of the model will benefit from experimental measurements of the current density distribution along the electrode surface, and many details remain to be elaborated in regard to the electrochemical mechanism by which the current density is increased in the scratch. Nonetheless, the approach described here offers a simple method for placing particles in desired locations on electrodes.

Acknowledgment. This work was supported by NASA OBPR, the NASA University Research, Engineering, and Technology Institute on BioInspired Materials (BIMat) under Award Nos. NCC-1-02037 and NSF/DMR-0213706, and ARO/MURI under Grant No. W911NF-04-1-0170. Partial support for W.D.R. was provided by NASA GSRP. C.P. acknowledges support by the Alexander von Humboldt Foundation.

Supporting Information Available: Solution for the stream function to leading order and definition of the constants C_1, C_2, K_1, K_2, and K_3. This material is available free of charge via the Internet at http://pubs.acs.org.

LA801419K